Phase evolution and field-induced magnetic anisotropy of the nanocomposite three-phase fcc, hcp, and amorphous soft magnetic alloy $Co_{89}Zr_7B_4$

P. R. Ohodnicki, Jr.,[1,a] V. Keylin,[2] H. K. McWilliams,[1] D. E. Laughlin,[1] and M. E. McHenry[1]

[1]*Materials Science and Engineering Department, Carnegie Mellon University, Pittsburgh, Pennsylvania 15213,USA*
[2]*Magnetics, Division of Spang & Company, Pittsburgh, Pennsylvania 15238, USA*

Crystallization and field-induced magnetic anisotropy were investigated for a $Co_{89}Zr_7B_4$ alloy. A mixture of nanocrystalline fcc and hcp phases surrounded by an amorphous matrix is present after primary crystallization. For annealing in a 2 T transverse field, the observed anisotropy fields and field-induced anisotropies are $H_K \sim 12-15$ Oe and $K_U \sim 550-680$ J/m^3 for field annealed amorphous ribbons as compared to $H_K \sim 18-19$ Oe and $K_U \sim 800-850$ J/m^3 for field crystallized ribbons. In comparison with the corresponding Fe-based alloy, the relatively high Curie temperature and large field-induced anisotropy of the field annealed amorphous ribbons indicate that the intergranular amorphous phase may provide a relatively more significant contribution to the field-induced anisotropy of Co-based nanocomposite ribbons such as $Co_{89}Zr_7B_4$. © *2008 American Institute of Physics.* [DOI: 10.1063/1.2839284]

Fe-based soft magnetic amorphous and nanocomposite materials can be engineered to simultaneously display low core losses, high saturation inductions, and low saturation magnetostrictions. The most commonly studied soft magnetic nanocomposites are derivatives of the Fe–Nb–Si–B–Cu Finemet (Ref. 1) and the Fe–Zr–B–(Cu) Nanoperm alloys.[2] To address the demand for soft magnetic materials for high frequency and high temperature applications, nanocomposites with large amounts of Co have been synthesized to achieve higher saturation inductions and better temperature stability of magnetic properties as in Fe–Co–Zr–B–Cu HiT-Perm alloys.[3,4] Additions of Co to Fe-based alloys are also expected to increase the field-induced magnetic anisotropy observed by thermomagnetic processing based on simple arguments from the directional pair ordering theory of induced magnetic anisotropy in binary alloys.[5,6] A large transverse field-induced anisotropy is of interest for applications requiring low core loss soft magnetic alloys with low permeabilities and linear *B-H* loops up to high fields.

Recently, the nanocrystallization and magnetic properties of Fe and Co based nanocomposite alloys with even larger Co contents have been investigated. Work on Co-rich Co–Fe–Nb–Si–B and Co–Fe–Zr–Si–B nanocomposite alloys has demonstrated a large field-induced anisotropy for Co-rich compositions with Co:Fe ratios ranging approximately between 0.8:0.2 and 0.9:0.1.[7,8] For a Co-rich Co–Fe–Zr–B alloy in Ref. 10, it was observed that a bcc nanocrystalline phase nucleated first at the lowest crystallization temperatures even though the Co:Fe ratio corresponded to the single phase fcc region of the binary Fe:Co phase diagram. To better understand the nanocrystallization and magnetic properties of high Co-containing soft magnetic nanocomposite al-

loys, a study of the phase evolution and field-induced magnetic anisotropy observed upon annealing a $Co_{89}Zr_7B_4$ amorphous alloy is presented here.

An amorphous ribbon of $Co_{89}Zr_7B_4$ composition was synthesized through single-roller wheel melt spinning with an overpressure of 1 psi of argon to eject the melt with a wheel velocity of approximately 25 m/s. For studies of the phase evolution, small pieces of the ribbon were encapsulated in sealed quartz tubes in an Ar atmosphere and isothermally annealed between 450 and 900 °C for 1 h followed by a water quench.

Roughly 2 m lengths of the as-cast amorphous ribbon were wound into toroidal cores and annealed at temperatures ranging from 350 to 530 °C for 1 h in flowing N$_2$ with or without a magnetic field of 2 T. The transverse field was applied at all times when the cores were at elevated temperatures. High temperature magnetization measurements were made using a Lakeshore high temperature vibrating sample magnetometer (VSM) with an average heating rate of ~ 4 °C/min. *B-H* loops were obtained for toroidal cores using a Walker AMH-401 hysteresisgraph. Constant heating rate differential scanning calorimetry (DSC) experiments were performed using a Perkin Elmer diamond DSC with heating and cooling rates of 40 °C/min.

A series of x-ray diffraction (XRD) patterns obtained from the $Co_{89}Zr_7B_4$ alloy is presented in Fig. 1 for 1 h isothermal annealing treatments of ribbon pieces. Broad crystalline peaks are observed in the XRD patterns after isothermal annealing at 450 and 500 °C resulting in primary crystallization. All of the observed peaks can be indexed by assuming that fine-grained fcc and hcp Co are present as primary crystallization products. For an isothermal annealing temperature of 600 °C, the onset of secondary crystallization of the remaining amorphous phase yields the appearance of additional XRD peaks indexed to both the Co_2Zr and $Co_{23}Zr_6$

---
[a]Author to whom correspondence should be addressed. Electronic mail: pohodnic@andrew.cmu.edu.
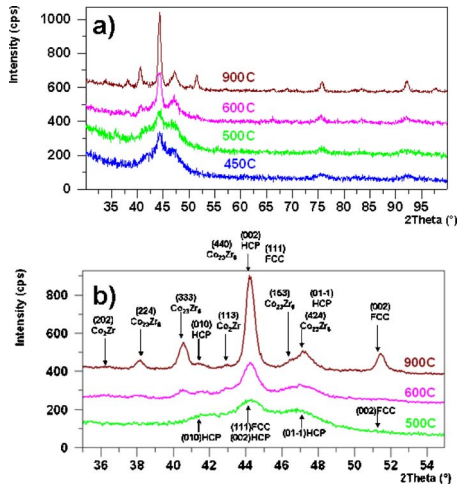
FIG. 1. (Color online) (a) XRD scans of isothermally annealed $Co_{89}Zr_7B_4$ samples as a function of annealing temperature and (b) longer scans over a shorter angular range with peaks labeled. Below secondary crystallization, a three-phase mixture of fcc, hcp, and amorphous phases is observed.

FIG. 3. (Color online) (a) Magnetization curves and (b) differential scanning calorimetry data that demonstrate no magnetic or thermal signature of a fcc to hcp transformation after heating and cooling of the crystallized ribbons.

phases. At high annealing temperatures (e.g., 900 °C), the XRD peak intensities suggest that the volume fraction of Co_2Zr decreases while the volume fraction of $Co_{23}Zr_6$ phase increases. This observation suggests that the Co_2Zr phase is metastable at this composition. The XRD peaks indexed to the hcp crystalline phase become sharper and relatively lower in intensity above secondary crystallization temperatures but these peaks are still observed even after the 900 °C annealing treatment.

A bright field transmission electron microscopy (TEM) image and a corresponding selected area diffraction pattern (SADP) of the ribbon annealed at 450 °C are presented in Fig. 2. The average grain size observed is smaller than 10 nm. Intensity corresponding to fcc ring patterns and relatively weak intensity corresponding to the hcp ring patterns are observed. The broad inner ring in the SADP consists of a superposition of five different rings (three hcp and two fcc rings) which are broadened due to the fine grain size and correspond to the superposition of broad peaks observed between $2\theta \sim 35°$ and $55°$ in the XRD data of Fig. 1.

High temperature VSM and DSC have been used to determine if both crystalline phases are present immediately after primary crystallization or if hcp phase forms on cooling from a nucleated fcc phase. Magnetization, $M(T)$, curves up to 540 °C for heating and cooling of an initially amorphous ribbon are presented in Fig. 3(a). On heating, a sharp drop in the magnetization is observed at $T \sim 462$ °C corresponding
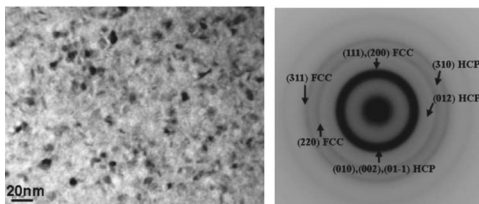
FIG. 2. Bright field image and corresponding selected area diffraction pattern illustrating the average grain size of less than 10 nm as well as diffraction intensity which suggests a three-phase mixture of fcc and hcp Co nanocrystals embedded within an amorphous matrix.
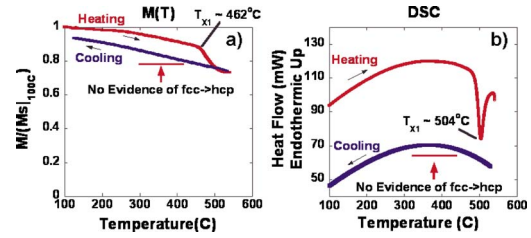
to the onset of primary crystallization (T_{X1}). As observed for $(Co_{1-x}Fe_x)_{89}Zr_7B_4$ and $(Co_{1-x}Fe_x)_{88}Zr_7B_4Cu_1$ alloys with small Fe additions ($x < \sim 0.10$), the primary crystalline phase exhibits a lower magnetization than the as-cast amorphous phase near the primary crystallization temperature. As a result, a magnetization drop at T_{X1} is observed in $M(T)$ data for initially amorphous ribbons.[9,10] In the case of bulk Co alloys, a discontinuous jump in magnetization is typically observed at the hcp↔fcc transformation temperatures which occur in the range of 350–450 °C due to the difference in saturation magnetization of the two phases.[11] Here, no magnetic signature of a phase transformation is observed on cooling the ribbons after heating to undergo primary crystallization.

The same experiment was performed using the DSC and the results are presented in Fig. 3(b). For these experiments, heating and cooling rates of 40 °C/min and an isothermal hold at 540 °C for 30 min after the initial heating to 540 °C were employed to ensure that primary crystallization is largely completed. On heating, the exothermic peak associated with primary crystallization is observed with a peak temperature of $T \sim 504$ °C. This temperature is larger than the onset temperature measured for the VSM data of Fig. 3(a) due to the difference in heating rates. Similar to VSM experiments, no thermal signature of a fcc to hcp transformation is observed on cooling. Therefore, it is proposed that both the fcc and hcp intensities observed in XRD and TEM are due to crystallites that form during primary crystallization. It is also reasonable to propose that both the hcp and fcc phases nucleate directly from the amorphous phase.

Transverse field annealing experiments were performed on amorphous $Co_{89}Zr_7B_4$ ribbons wound into toroidal cores to measure the magnitude of field-induced magnetic anisotropy. Assuming the field-induced anisotropy to be uniaxial with the easy axis along the direction of the annealing field, the uniaxial anisotropy constant K_U is estimated from the measured anisotropy field H_K of hysteresis loops according to $K_U = H_K M_S / 2$. Here, estimates of H_K were obtained by extrapolating the low field linear magnetization loop to the saturation induction for dynamic *B-H* loops measured at $f = 3$ kHz and the values of M_S were obtained independently from a VSM.

Figure 4 shows dynamic *B-H* loops and the corresponding values of H_K and H_C. Ribbons field annealed at 450 °C are still amorphous in contrast to samples that were encapsulated and annealed to obtain the XRD data of Fig. 1. This
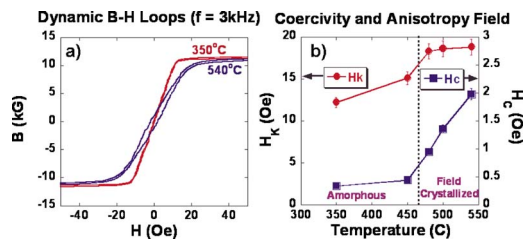
FIG. 4. (Color online) (a) Dynamic *B-H* loops obtained for $Co_{89}Zr_7B_4$ ribbons field annealed at several different temperatures and (b) a plot of anisotropy field and coercivity estimated from these loops.

contradiction is due to the close proximity of the annealing temperature to T_{X1} and differences in the temperature profile of the furnaces used to carry out these treatments. It is clear from Fig. 4 that field annealing of the as-cast amorphous ribbons at temperatures too low for primary crystallization still results in significant anisotropy fields ($H_K \sim 12-15$ Oe) that increase with increasing annealing temperature. Samples treated in this way are referred to as field annealed amorphous ribbons. The field crystallized ribbons exhibit H_K values ($H_K \sim 18-19$ Oe) which are not strongly annealing temperature dependent and are slightly higher than the highest H_K measured here for the field annealed amorphous ribbon. Because the M_S values are only reduced slightly after crystallization of the amorphous ribbons, estimates of K_U show roughly the same trend as H_K plotted in Fig. 4. We estimate $K_U \sim 550-680$ J/m^3 for the field annealed amorphous ribbons investigated here and $K_U \sim 800-850$ J/m^3 for the field crystallized ribbons. The K_U values for the field crystallized nanocomposite $Co_{89}Zr_7B_4$ alloy are significantly larger than those for the corresponding Fe-based alloys ($K_U \sim 80$ J/m^3 in nanocrystallized $Fe_{90}Zr_7B_3$ as reported in Ref. 6). Despite the presence of a nanocrystalline hcp phase with a large uniaxial magnetocrystalline anisotropy after primary crystallization, no evidence for an in-plane crystallographic texture is observed in the ring patterns of selected area diffraction patterns obtained from field crystallized samples.

Figure 4 indicates an increase in dynamic coercivity ($f = 3$ kHz) at field annealing temperatures sufficiently high for crystallization. The increase in coercivity may be related to the relatively large magnetocrystalline anisotropies of the crystalline phases present after primary crystallization.[12] Despite the clear increase in dynamic coercivity (H_C) with increasing field crystallization temperatures, the measured anisotropy fields (H_K) do not show an experimentally significant trend with field crystallization temperature.

For the Co–Zr–B alloy investigated here, the observation of only nanocrystalline fcc and hcp phases present after primary crystallization shows that Fe is required in order to observe bcc phase as a primary crystallization product in nanocrystalline alloys of $(Co_{1-x}Fe_x)_{89}Zr_7B_4$ composition after 1 h isothermal annealing temperatures near T_{X1}. This observation is important as a tendency for bcc phase to nucleate first has been demonstrated even in an alloy containing very little Fe.[10] For the alloy studied here, formation of nanocrystals of two ferromagnetic transition metal rich primary crystalline phases (fcc and hcp) for an alloy with only one ferromagnetic transition metal element is interesting from the standpoint of the thermodynamics and kinetics governing nucleation of the primary crystalline phase in the Co-rich nanocomposites.

The magnitudes of the field-induced anisotropies observed for the field crystallized $Co_{89}Zr_7B_4$ ribbons are larger than those observed for the corresponding Fe-based ribbons.[6] The field-induced anisotropy of the Fe-based ribbon of Ref. 6 was claimed to be associated with small amounts of dissolved Zr or B atoms in the nanocrystalline phase. For the Co-based alloy, the same mechanism is expected to be active as well. In addition, a hcp phase with high uniaxial magnetocrystalline anisotropy is present but no clear evidence of crystallographic texture due to field annealing has been observed. For the Co-based alloy, the field annealed amorphous ribbons exhibited field-induced anisotropies only slightly less than those for field crystallized ribbons. Because of the high Curie temperature and the relatively high field-induced anisotropy observed in field annealed amorphous ribbons, the intergranular amorphous phase is likely to play a more significant role in the observed field-induced magnetic anisotropies for the Co-based nanocomposites such as $Co_{89}Zr_7B_4$.

XRD and TEM show $Co_{89}Zr_7B_4$ ribbons to exhibit a three-phase microstructure of fcc and hcp nanocrystalline phases embedded in an amorphous matrix after primary crystallization. Toroidal cores wound from $Co_{89}Zr_7B_4$ ribbons exhibited anisotropy fields of $H_K \sim 12-15$ Oe for field annealed amorphous ribbons and $H_K \sim 18-19$ Oe for field crystallized ribbons. The field-induced anisotropies are larger than those observed for the corresponding Fe-based alloys. No evidence of in-plane crystallographic texture was identified by TEM. Because of the high Curie temperature and the relatively large field-induced anisotropies observed for field annealed amorphous ribbons of Co-based compositions, the amorphous phase is likely to provide a more significant contribution to the overall field-induced anisotropy of the nanocomposites as compared to the corresponding Fe-based compositions.

[1] Y. Yoshizawa and K. Yamuchi, *Magnetic Properties of Nanocrystalline Fe-Based Soft Magnetic Alloys*, MRS Symposia Proceedings Vol. 232 (Materials Research Society, Pittsburgh, PA, 1990), pp. 183–192.
[2] K. Suzuki *et al.*, Mater. Trans., JIM **31**, 743 (1990).
[3] M. A. Willard, D. E. Laughlin, M. E. McHenry, D. Thoma, K. Sickafus, J. O. Cross, and V. G. Harris, J. Appl. Phys. **84**, 6773 (1998).
[4] M. E. McHenry, M. A. Willard, and D. E. Laughlin, Prog. Mater. Sci. **44**, 291 (1999).
[5] S. Chikazumi, *Physics of Ferromagnetism* (Clarendon, Oxford, 1997).
[6] K. Suzuki, N. Ito, J. S. Garitaonandia, and J. D. Cashion, J. Appl. Phys. **99**, 08F114 (2006).
[7] Y. Yoshizawa, S. Fujii, D. H. Ping, M. Ohnuma, and K. Hono, Scr. Mater. **48**, 863 (2003).
[8] Y. Yoshizawa, S. Fujii, D. H. Ping, M. Ohnuma, and K. Hono, Mater. Sci. Eng., A **375–377**, 207 (2004).
[9] P. R. Ohodnicki, S. Y. Park, H. K. McWilliams, K. Ramos, D. E. Laughlin, and M. E. McHenry, J. Appl. Phys. **101**, 09N108 (2007).
[10] M. A. Willard, T. M. Heil, and R. Goswami, Metall. Mater. Trans. A **38**, 725 (2007).
[11] R. C. O'Handley, B. W. Corb, and N. J. Grant, J. Appl. Phys. **55**, 1808 (1984).
[12] X. B. Liang *et al.*, Physica B **370**, 151 (2005).